
Near-Field Antenna Characterization Through a Compressive Sensing Based Approach

M. Salucci, N. Anselmi, and A. Massa

December 22, 2019

Contents

1	Glossary	3
2	Mathematical Formulation and Definitions	5
3	Near-Field Antenna Characterization Through the Orthogonal Matching Pursuit (OMP) Approach	11

1 Glossary

- AUT : Antenna Under Test;
- $\underline{\underline{A}}_b$, $b = 1, \dots, B$: Pattern matrix of the b -th class of defects;
- $\underline{\underline{A}}_b^{(k)}$, $k = 1, \dots, K$: Vector of near-field measurements considering all the T interpolation points;
- $\underline{\underline{U}}_b$, $b = 1, \dots, B$: Unitary matrix whose columns are called *left-singular vectors* of $\underline{\underline{A}}_b$;
- $\underline{\underline{\Sigma}}_b$, $b = 1, \dots, B$: Diagonal matrix whose entries are the singular values of $\underline{\underline{A}}_b$;
- $\underline{\underline{V}}_b$, $b = 1, \dots, B$: Unitary matrix whose columns are called *right-singular vectors* of $\underline{\underline{A}}_b$;
- B : Number of considered classes of defects affecting the AUT to build the over-complete basis;
- η : Threshold on the singular values;
- Q_b : Number of singular values above threshold for the b -th class of defects;
- $Q = \sum_{b=1}^B Q_b$: Total number of vectors in the over-complete basis;
- K_b : Total number of simulated AUT configurations for the b -th class of defects;
- $K = \sum_{b=1}^B K_b$: Total number of simulated AUT configurations to build the over-complete basis;
- \underline{y} : Vector of near-field measurements of the AUT ;
- OMP : Orthogonal Matching Pursuit;
- \mathcal{I} : Maximum number of iterations performed by the OMP algorithm;
- \mathcal{Z} : Subset of indexes of the selected columns of the basis $\underline{\underline{L}}$;
- \underline{r} : Residual of OMP algorithm;
- \underline{Corr} : Correlation vector of the OMP algorithm;
- S : Number of subarrays;
- N : Total number of antenna elements;
- N_x : Number of elements in each row of the antenna array;
- N_y : Number of elements in each column of the antenna array;
- $N^{(s)}$: Number of antenna elements belonging to the s -th subarray ($s = 1, \dots, S$);
- $\mathbf{r}_n^{(s)} = (x_n^{(s)}, y_n^{(s)}, z_n^{(s)})$: Position of the n -th element in the s -th subarray ($n = 1, \dots, N^{(s)}$; $s = 1, \dots, S$);
- $L_{x/y}$: Total antenna dimension along x/y ;
- $d_{x/y}$: Spacing along x/y between elements in the array;

-
- M : Number of measurement points;
 - $\mathbf{r}_m = (x_m, y_m, z_m)$: Position of the m -th measurement points ($m = 1, \dots, M$);
 - $\Delta_{x/y}^{meas}$: Measurement step along x/y ;
 - T : Number of interpolation points ($T \gg M$);
 - $\mathbf{r}_t = (x_t, y_t, z_t)$: Position of the t -th interpolation point ($t = 1, \dots, T$);
 - $\Delta_{x/y}^{int}$: Interpolation step along x/y ;
 - H : Height of the near-field measurement/interpolation region;
 - $w_n^{(s)} = \alpha_n^{(s)} \exp(j\beta_n^{(s)})$: Complex excitation of the n -th element belonging to the s -th subarray;
 - $\nu^{(s)}$: Magnitude failure factor of the excitations of the elements of the s -th subarray;
 - $F^{(s)}$: Total number of failure factors considered for the elements in the s -th subarray;
 - $F = \sum_{s=1}^S F^{(s)}$: Total number of failure factors considered to build the over-complete basis;
 - $\gamma^{(s)}$: Phase failure of the excitations of the elements of the s -th subarray;
 - $P^{(s)}$: Total number of phase failures considered for the elements in the s -th subarray;
 - $P = \sum_{s=1}^S P^{(s)}$: Total number of phase failures considered to build the over-complete basis;
 - I : Number of iterations performed by the *OMP* algorithm (corresponds to the number of selected vectors in the over-complete basis);
 - l_{dip} : Length of the dipoles;
 - r_{dip} : Radius of the dipoles;
 - h_{gnd} : Height of dipoles above the ground plane;
 - $L_{x/y}^{(s)}$: Size of the s -th subarray along x/y , $s = 1, \dots, S$;
 - ζ_{meas} : Length of the (reduced) measurement plane side;
 - ζ_{int} : Length of the full measurement plane side;

2 Mathematical Formulation and Definitions

The measurement plane is defined inside the near-field region of the *AUT* where T (~ 1000) measurement points are evenly distributed. However, for the measurement of the *AUT* near-field just $M \ll T$ measurement points are employed.

The Measurement-by-Design framework can be described as a 4 – *steps* algorithm:

1. Pattern matrices creation;
2. Truncated-Singular Value Decomposition (T-SVD) of the pattern matrices;
3. Construction of the “Over-Complete basis”;
4. Application of a Compressive Sensing algorithm.

Pattern Matrices Creation

Primarily, by taking into account available *a priori* information, B classes of uncertainties are identified, where an uncertainty is whatever imperfection that could affect either the *AUT*, due to manufacturing flaws, or the measurement set-up, due to improper positioning of the *AUT* or the measurement plane, causing a deviation of the *AUT* radiated features from the nominal ones. For each class of uncertainties $b = 1, \dots, B$, K_b simulations are performed considering different values of the uncertainty parameter whose variation range is pre-defined according to accessible *a priori* information.

Each simulation gives as output a field pattern $\underline{A}_b^{(k)}$; all the $\underline{A}_b^{(k)}$, $k = 1, \dots, K_b$ patterns related to a certain uncertainty class $b = 1, \dots, B$ are then put together in order to build the related pattern matrix $\underline{\underline{A}}_b \in \mathbb{C}^{T \times K_b}$:

$$\underline{\underline{A}}_b = [\underline{A}_b^{(1)}, \underline{A}_b^{(2)}, \dots, \underline{A}_b^{(K_b)}], \quad b = 1, \dots, B \quad (1)$$

where

- $\underline{A}_b^{(k)} \in \mathbb{C}^{T \times 1}$, $k = 1, \dots, K$ is the vector of near-field measurements related to the k – *th* uncertainty parameter value of the b – *th* uncertainty class, which is built considering all the T points of the measurement plane.

Truncated-Singular Value Decomposition (T-SVD) of the pattern matrices

At this point all $\underline{\underline{A}}_b$, $b = 1, \dots, B$ pattern matrices are created. To each $\underline{\underline{A}}_b$, $b = 1, \dots, B$ the T-SVD is applied considering a certain threshold η on the singular values. Mathematically:

- Singular Value Decomposition :

$$\underline{\underline{A}}_b = \underline{\underline{U}}_b \underline{\underline{\Sigma}}_b \underline{\underline{V}}_b^T, \quad b = 1, \dots, B \quad (2)$$

where

- $\underline{\underline{U}}_b \in \mathbb{C}^{T \times T}$ is a unitary matrix whose columns are called *left-singular vectors* of $\underline{\underline{A}}_b$;
- $\underline{\underline{\Sigma}}_b \in \mathbb{R}^{T \times K}$ is a diagonal matrix whose entries are the singular values of $\underline{\underline{A}}_b$;
- $\underline{\underline{V}}_b \in \mathbb{C}^{K \times K}$ is a unitary matrix whose columns are called *right-singular vectors* of $\underline{\underline{A}}_b$;

– \underline{V}_b^T is the conjugate transpose of \underline{V}_b .

By applying the truncation at the considered threshold η :

$$\underline{\hat{A}}_b = \underline{\hat{U}}_b \underline{\hat{\Sigma}}_b \underline{\hat{V}}_b^T, \quad b = 1, \dots, B \quad (3)$$

where

- $\underline{\hat{U}}_b \in \mathbb{C}^{T \times Q_b}$;
- $\underline{\hat{\Sigma}}_b \in \mathbb{R}^{Q_b \times Q_b}$;
- $\underline{\hat{V}}_b^T \in \mathbb{C}^{Q_b \times K}$;
- Q_b is the number of singular values above threshold for the b -th class of defects;

Construction of the Dictionary

The “Over-Complete basis” (also called *Dictionary*, \underline{D}) is then constructed by putting together the $\underline{\hat{U}}_b$, $b = 1, \dots, B$ matrices :

$$\underline{D} = [\underline{\hat{U}}_1, \underline{\hat{U}}_2, \dots, \underline{\hat{U}}_B] \in \mathbb{C}^{T \times (Q_1 + \dots + Q_B)} \quad (4)$$

From the over-complete basis \underline{D} just the M rows related to the $M \ll T$ used measurements points are considered, obtaining : $\underline{L} \in \mathbb{C}^{M \times (Q_1 + \dots + Q_B)}$. Thus, the problem can be formulated as follows: starting from the knowledge of the measured near-field of the AUT ($\underline{y} \in \mathbb{C}^{M \times 1}$), the objective is to find the vector of coefficients \underline{x} such that :

$$\underline{L} \underline{x} \simeq \underline{y} \quad (5)$$

where

- \underline{x} is the problem solution, which indicates what combination of the vectors of \underline{L} (i.e. what combination of defects) allows to better approximate the data \underline{y} .

Compressive Sensing algorithm application

Being \underline{x} sparse (meaning that just few of its elements are non-zero), it is possible to find a solution for the problem described in (5) applying *Compressive Sensing* (CS) approaches such as :

- *Orthogonal Matching Pursuit* (OMP);
- *Bayesian Compressive Sensing* (BCS).

Orthogonal Matching Pursuit (OMP)

The *OMP* is a *sparse approximation* algorithm which involves finding the “best matching ” projections of data onto the span of an over-complete dictionary. The main features that makes this method advantageous in signal recovery problems are its speed and its ease of implementation. More in detail, remembering the problem at hand (5), the *OMP* is an iterative greedy algorithm that selects at each iteration the basis function (i.e. the column) of the basis of $\underline{\underline{L}}$ which presents the highest correlation with the current residual. This column is then joined into the set of selected columns. After the update of the residuals by means of the projection of the observation \underline{y} onto the linear subspace spanned by the columns that have already been selected, the algorithm iterates. It is worth to note that, since in the *OMP* algorithm the same column cannot be selected twice, at each iteration the residuals are orthogonal to all the selected columns of $\underline{\underline{L}}$ and whose set grows at each iteration.

The *OMP* algorithm can be enunciated as follows:

Let's assume that the columns of $\underline{\underline{L}}$ are normalized so that $\|\underline{\underline{L}}_j\|_2 = 1$ for $j = 1, \dots, \mathcal{J}$, with $\mathcal{J} = (Q_1 + \dots + Q_B)$. For any subset $\mathcal{Z} \subseteq \{1, 2, \dots, \mathcal{J}\}$, indicate with $\underline{\underline{L}}(\mathcal{Z})$ a submatrix of $\underline{\underline{L}}$ consisting of the columns $\underline{\underline{L}}_j$ with $j \in \mathcal{Z}$.

- *Step 0*: Fix the maximum number of iterations \mathcal{I} ;
- *Step 1*: Initialize the *residual* \underline{r}_0 equal to the data \underline{y} , $\underline{r}_0 = \underline{y}$, and initialize the set of selected columns $\underline{\underline{L}}(z_0) = \emptyset$. Set the iteration index $i = 1$;
- *Step 2*: Find the column $\underline{\underline{L}}_j$ of the basis $\underline{\underline{L}}$ that obtains the maximum correlation with the residual

$$\max_j |\underline{\underline{L}}_j^T \underline{r}_{i-1}| \quad (6)$$

being T the transpose operator, putting the correlation to zero for those indexes that have been already selected, in order to avoid that they are selected again. Add the suitable column $\underline{\underline{L}}_j$ to the set of selected columns. Update $z_i = z_{i-1} \cup \{j\}$.

- *Step 3*: Compute the projection matrix

$$\underline{\underline{P}}_i = \underline{\underline{L}}(z_i) [\underline{\underline{L}}(z_i)^T \underline{\underline{L}}(z_i)]^{-1} \underline{\underline{L}}(z_i)^T \quad (7)$$

and calculate the projection of the data onto the linear space spanned by the elements of $\underline{\underline{L}}(z_i)$; then, update the residual

$$\underline{r}_i = (\underline{I} - \underline{\underline{P}}_i) \underline{y} \quad (8)$$

where \underline{I} denotes the identity matrix.

- *Step 4*: if the termination criteria is reached, stop the algorithm. Otherwise, augment the iteration index $i = i + 1$ and repeat from *Step 2*.

One of the fundamental elements of an iterative scheme like *OMP* is the stopping rule. In the noiseless case the understandable termination criteria is $\underline{r}_i = 0$. That is, the algorithm stops whenever $r_i = 0$ is achieved. However, usually

measurements are noisy preventing the adoption of the aforementioned stopping criteria. Therefore in this work, where measurements are supposed to be affected by zero-mean Gaussian noise, the chosen termination rule is the achievement of a prefixed maximum number of iterations. Even if the considered stopping rule is very simple, the selection of a suitable maximum number of iterations is not straightforward because it cannot be made *a priori* and requires an empirical approach in order to avoid a surplus of iterations which results only in a waste of time and resources.

Near-Field Matching Error

The following integral error is defined to compute the mismatch between the actual and the retrieved field distribution radiated by the *AUT* evaluated over a grid of $T = 41 \times 41 = 1681 \frac{\lambda}{2}$ equi-spaced points on the measurement plane

$$\Xi_{AUT} = \frac{\sum_{t=1}^T |E_{AUT}(\mathbf{r}_t) - \tilde{E}_{AUT}(\mathbf{r}_t)|^2}{\sum_{t=1}^T |E_{AUT}(\mathbf{r}_t)|^2} \quad (9)$$

where

- $E_{AUT}(\mathbf{r}_t)$: actual field radiated by the *AUT*;
- $\tilde{E}_{AUT}(\mathbf{r}_t)$: estimated field radiated by the *AUT*;

Moreover, the difference between the field generated by the gold antenna (without defects) and by the *AUT* (with defects) is quantified by means of the following integral error

$$\Xi_{GOLD} = \frac{\sum_{t=1}^T |E_{GOLD}(\mathbf{r}_t) - E_{AUT}(\mathbf{r}_t)|^2}{\sum_{t=1}^T |E_{GOLD}(\mathbf{r}_t)|^2} \quad (10)$$

where

- $E_{GOLD}(\mathbf{r}_t)$: actual field radiated by the gold antenna.

Far-Field Matching Error

The following integral error is defined to compute the mismatch between the actual and the estimated far-field pattern of the *AUT*

$$\chi_{AUT} = \frac{\sum_u \sum_v |E_{AUT}(u, v) - \tilde{E}_{AUT}(u, v)|^2}{\sum_u \sum_v |E_{AUT}(u, v)|^2} \quad (11)$$

where

- $E_{AUT}(u, v)$: actual far-field pattern radiated by the *AUT*;
- $\tilde{E}_{AUT}(u, v)$: estimated far-field pattern radiated by the *AUT*;
- $u = \sin\theta \cos\varphi$;
- $v = \sin\theta \sin\varphi$;

Unless differently specified, the error is computed for all (u, v) points falling in the visible range

$$(u^2 + v^2) \leq 1 \quad (12)$$

Signal-to-Noise Ratio

Near-field measurements are corrupted by an additive white Gaussian noise with a signal-to-noise ratio equal to

$$SNR = 10 \log_{10} \left\{ \frac{\sum_{m=1}^M |E_{AUT}(\mathbf{r}_m)|^2}{\sum_{m=1}^M |\iota(\mathbf{r}_m)|^2} \right\} \quad (13)$$

where

- $E_{AUT}(\mathbf{r}_m)$: field radiated by the *AUT*;
- $\iota(\mathbf{r}_m)$: noise sample at position $\mathbf{r}_m = (x_m, y_m, z_m)$.

3 Near-Field Antenna Characterization Through the Orthogonal Matching Pursuit (OMP) Approach

Parameters

Gold Antenna (Without Defects)

- Geometry : Planar array of microstrip patches on the (x, y) plane;
- Working Frequency : $f = 3.6 [GHz]$ ($\lambda = 83.27 \times 10^{-3} [m]$ in free space);
- Substrate (PEC-backed) :
 - Dimensions : infinite;
 - Relative Permittivity : $\varepsilon_{r,sub} = 4.7$;
 - Loss Tangent : $\tan \delta_{sub} = 0.014$;
 - Thickness : $h_{sub} = 0.019 [\lambda]$ ($1.6 [mm]$);
- Microstrip patches :
 - Dimensions : $l_x \approx 0.22 [\lambda]$ ($18.16 [mm]$), $l_y \approx 0.33 [\lambda]$ ($27.25 [mm]$);
 - Feeding : pin-fed;
- Spacing between elements : $d_x = d_y = \frac{\lambda}{2}$;
- Number of elements in each row : $N_x = 6$;
- Number of elements in each column : $N_y = 10$;
- Total number of elements : $N = (N_x \times N_y) = 60$;
- Total size of the antenna : $L_x = 5 [\lambda]$, $L_y = 9 [\lambda]$;
- Element excitations : $w_n^{(s)} = 1.0 + j0.0$, $n = 1, \dots, N^{(s)}$, $s = 1, \dots, S$;

Antenna Under Test (AUT - With Defects)

1. Failures of the excitation magnitude of the 3^{rd} row;
 - Failure factor of the elements in the 3^{rd} row ($s = 3$) : $\nu^{(3)} = 0.45$;
2. Failures of the excitation phase of the 3^{rd} row;
 - Phase shift of the elements in the 3^{rd} row ($s = 3$) : $\gamma^{(3)} = \frac{\pi}{3} [rad]$;

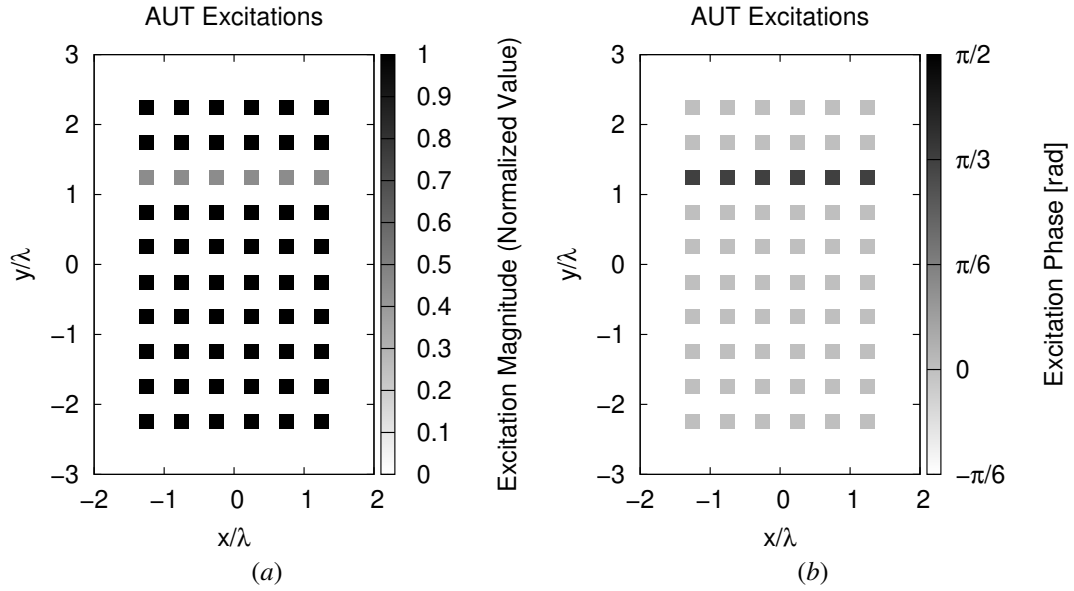


Figure 1: (a) Magnitude of the element excitations in the AUT ($\nu^{(3)} = 0.45$), (b) phase of the element excitations in the AUT ($\gamma^{(3)} = \frac{\pi}{3}$ [rad]).

Measurement Set-Up

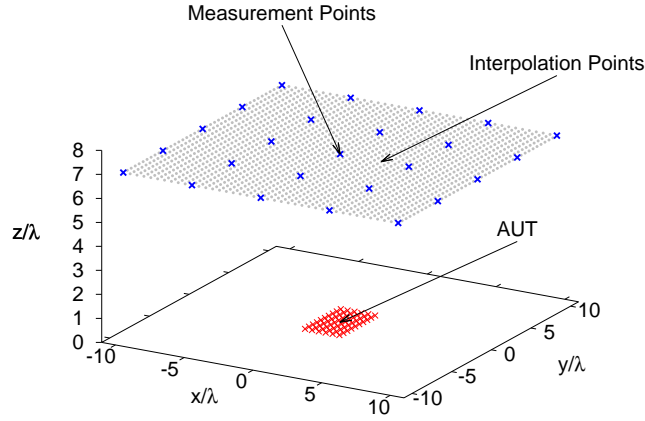


Figure 2: Disposition of the interpolation points ($T = 1681$) and of the measurement points ($M = 25$) in the near-field region of the AUT

- Type of measurements : near-field;
- Height of the measurement region : $H = 7$ [λ];
- Interpolation points :
 - Number of points : $T = 41 \times 41 = 1681$;
 - Coordinates : $x_t \in [-10, 10]$ [λ], $y_t \in [-10, 10]$ [λ], $z_t = H$ [λ], $t = 1, \dots, T$;
 - Interpolation step : $\Delta_{x/y}^{int} = 0.5$ [λ];
- Measurement points :
 - Coordinates : $x_m^{meas} \in [-10, 10]$ [λ], $y_m^{meas} \in [-10, 10]$ [λ], $z_m^{meas} = H$ [λ], $m = 1, \dots, M$;

-
- Number of points : $M_{x/y} = 5 \rightarrow M = 25$;
 - Measurement step : $\Delta_{x/y}^{meas} = 5 [\lambda]$
 - Ratio between number of measurements and total number of elements : $(M/N) = 0.42$;

Measurement-by-Design Technique

- Number of generated bases : $B = 20$;
- Bases $b = 1, \dots, 10$: magnitude failures in each row ($s = 1, \dots, 10$)
 - Failure factor of the elements : $\nu^{(s)} \in [0.0, 0.5]$, $s = 1, \dots, 10$;
 - Number of simulated failure factors : $F^{(s)} = 7$, $s = 1, \dots, 10$;
- Bases $b = 11, \dots, 20$: phase failures in each row ($s = 1, \dots, 10$)
 - Phase shift of the elements : $\gamma^{(s)} \in [0, \frac{\pi}{4}] [rad]$, $s = 1, \dots, 10$;
 - Number of simulated phase shifts: $P^{(s)} = 5$, $s = 1, \dots, 10$;
- Threshold on the singular values magnitude (normalized) : $\eta = -40 [dB]$;
- Total number of simulated *AUT* configurations : $K = S \times (F^{(s)} + P^{(s)}) = 10 \times (7 + 5) = 120$;

Noise

- *SNR* on the measured data : $SNR = \{50; 40; 30; 20; 10\} [dB]$;
- Noise seed : $Noise_Seed = 11$.

Near-Field Pattern of the Gold Antenna and of the AUT

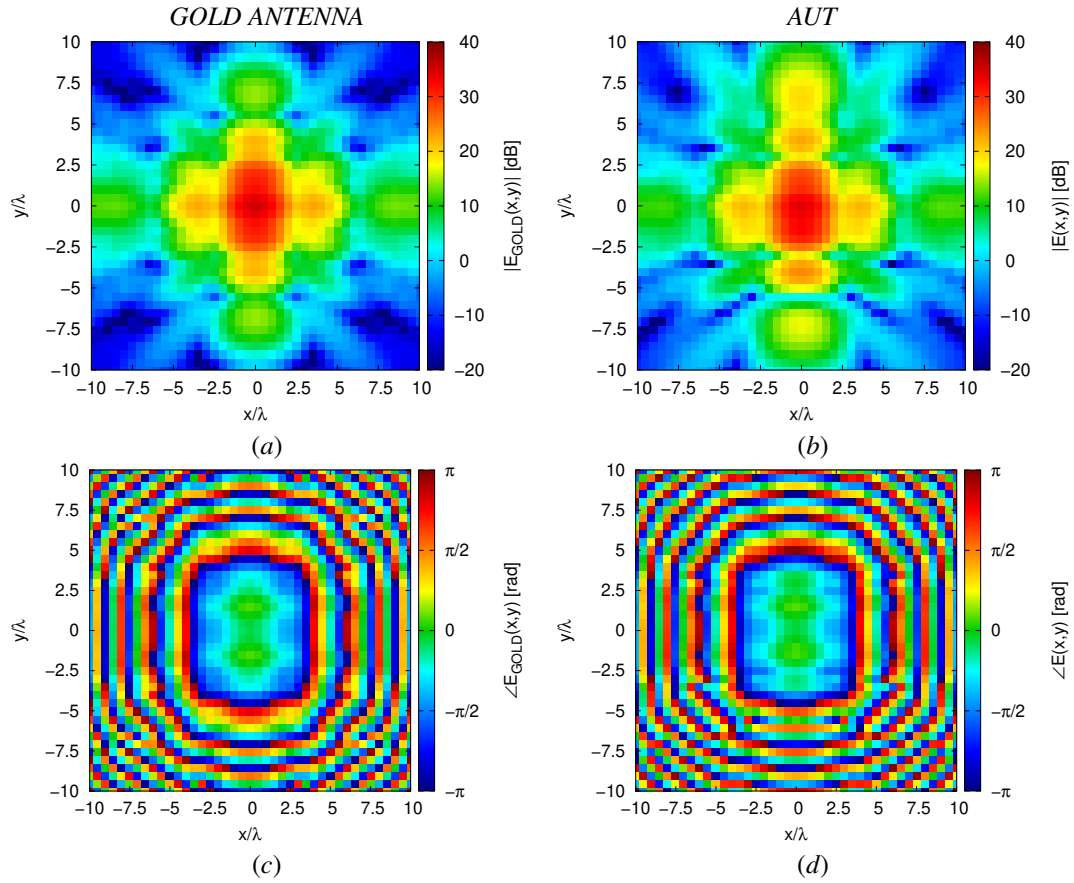


Figure 3: (a)(b) Magnitude and (c)(d) phase of the 2 – D near-field pattern radiated by (a)(c) the gold antenna and (b)(d) the AUT ($\nu^{(3)} = 0.45$, $\gamma^{(3)} = \frac{\pi}{3}$ [rad])

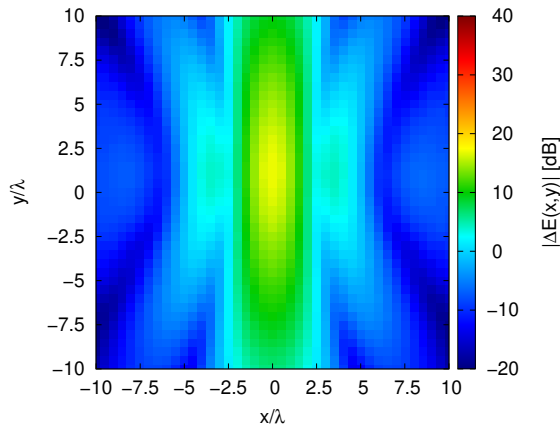


Figure 4: Magnitude of the difference between the 2 – D near-field pattern radiated by the gold antenna and the AUT ($\nu^{(3)} = 0.45$, $\gamma^{(3)} = \frac{\pi}{3}$ [rad]).

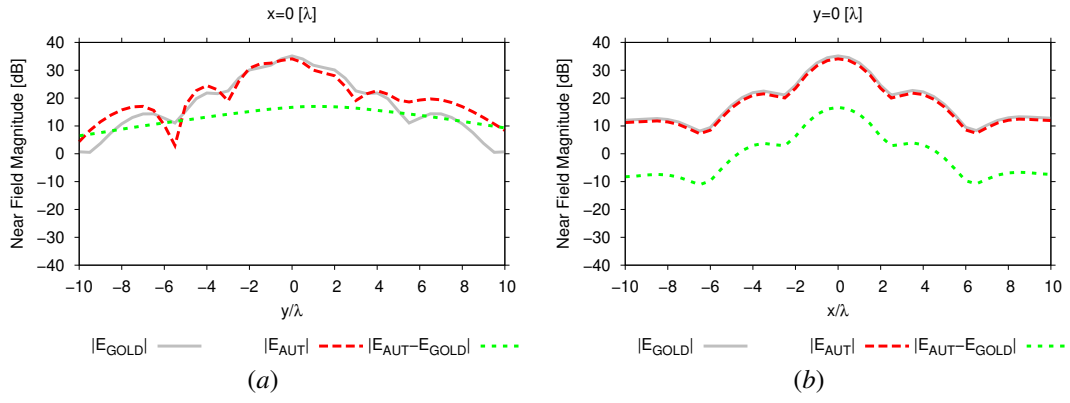


Figure 5: 1 – D cuts for (a) $x = 0 [\lambda]$ and (b) $y = 0 [\lambda]$ of the near-field magnitude radiated by the gold antenna and by the AUT ($\nu^{(3)} = 0.45, \gamma^{(3)} = \frac{\pi}{3} [rad]$).

The near-field matching error between the gold antenna and the AUT is equal to

$$\Xi_{GOLD} = 6.04 \times 10^{-2}.$$

Dimension of the Over-Complete Basis

The dimension of the over-complete basis is

$$Q = 40$$

This number is given by the sum of the vectors belonging to the two considered bases:

1. Magnitude failures : $Q_1, \dots, Q_{10} = 2$;
2. Phase failures : $Q_{11}, \dots, Q_{20} = 2$.

OMP Algorithm

Parameters

- Max. number of iterations of the *OMP* algorithm : $I = \{1; 2; 3; \dots; 10\}$;
- Selected iteration to report the results: $I = 5$; this choice is justified by the fact that at this iteration the *OMP* algorithm reaches the best near field error as shown in the following Fig. 6.

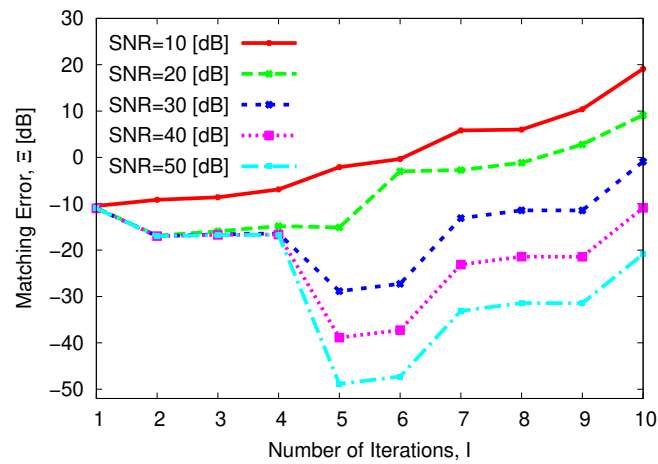


Figure 6: Behaviour of the near-field matching error versus the number of *OMP* iterations, I .

Results

Behaviour of the Near-Field Error

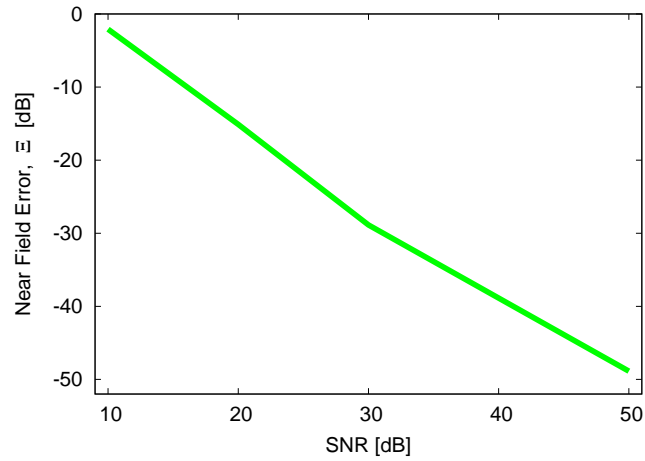


Figure 7: Near-Field Error behaviour versus SNR values

SNR [dB]	Ξ [dB]
50	-48.86
40	-38.86
30	-28.86
20	-15.11
10	-2.08

Table I: Near-field error obtained at different SNR values

Observations

- For $SNR \leq 20$ [dB] the near field error is quite high, but starting from $SNR \geq 30$ [dB] the *OMP* algorithm obtains good results and seems to follow a linear trend since its error decreases linearly as the SNR value increases.

Which vectors in the over-complete basis have been selected?

The following Fig. 8 shows which vectors of the over-complete basis (consisting of a total of $Q = 40$ vectors) have been selected in the first 5 *OMP* iterations ($i = 1, \dots, 5$). The goal is to understand if the *OMP* algorithm selects (and when) the vectors that are associated to a failure of the 3^{rd} row.

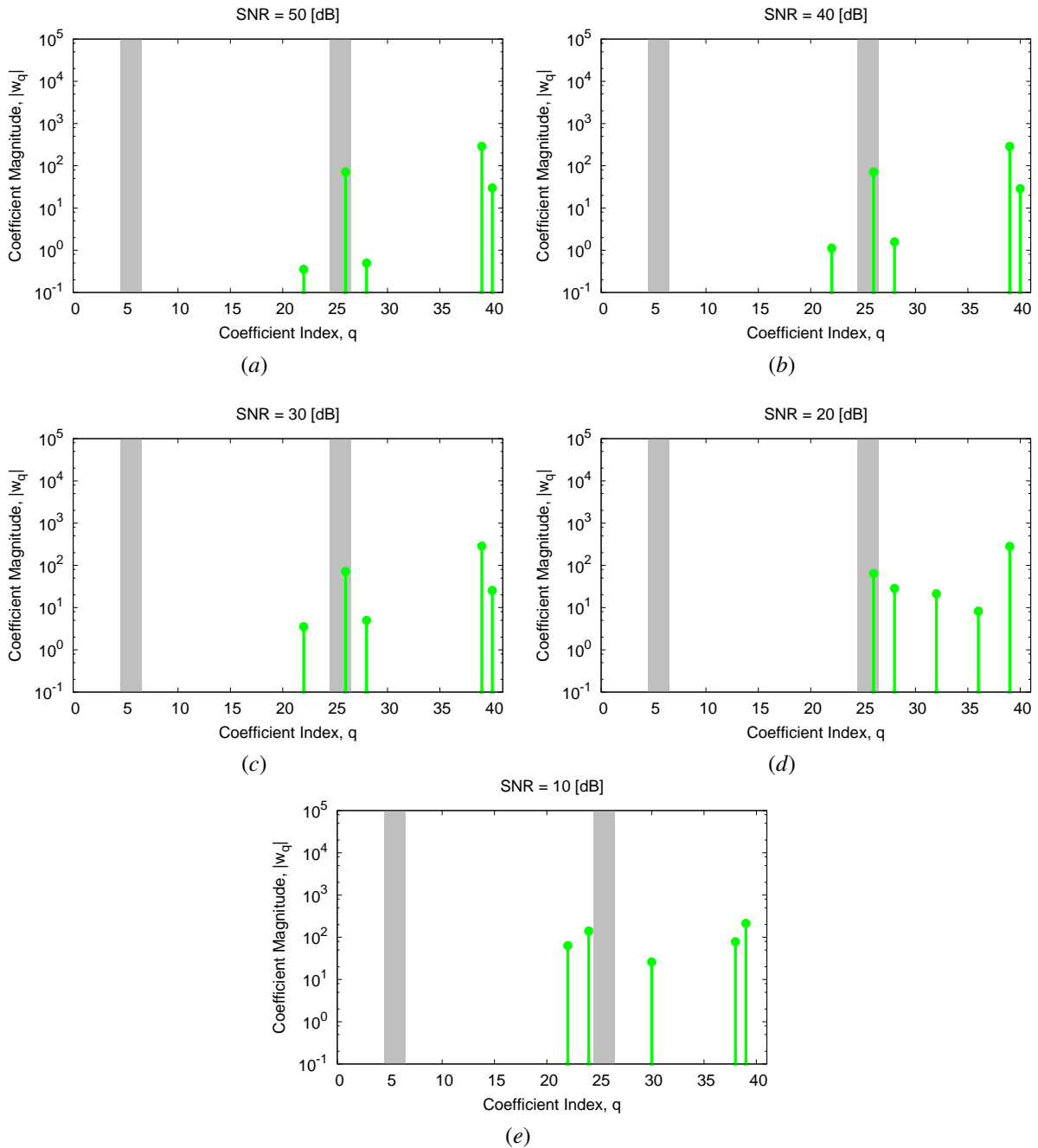


Figure 8: Selected coefficients by the *OMP* solver until the iteration $I = 5$

Observations

- Even if the measured *AUT* has a failure of the excitation magnitude of the 3^{rd} row, none of the vectors belonging to the magnitude failures has been selected in the first *OMP* iterations;
- The *OMP* solver is able to detect the phase failure affecting the *AUT* for $SNR \geq 20$ [dB];

-
- In the case of $SNR = 30 [dB]$, $SNR = 40 [dB]$ and $SNR = 50 [dB]$ the same vectors have been selected in the same order.

Estimated Near-Field

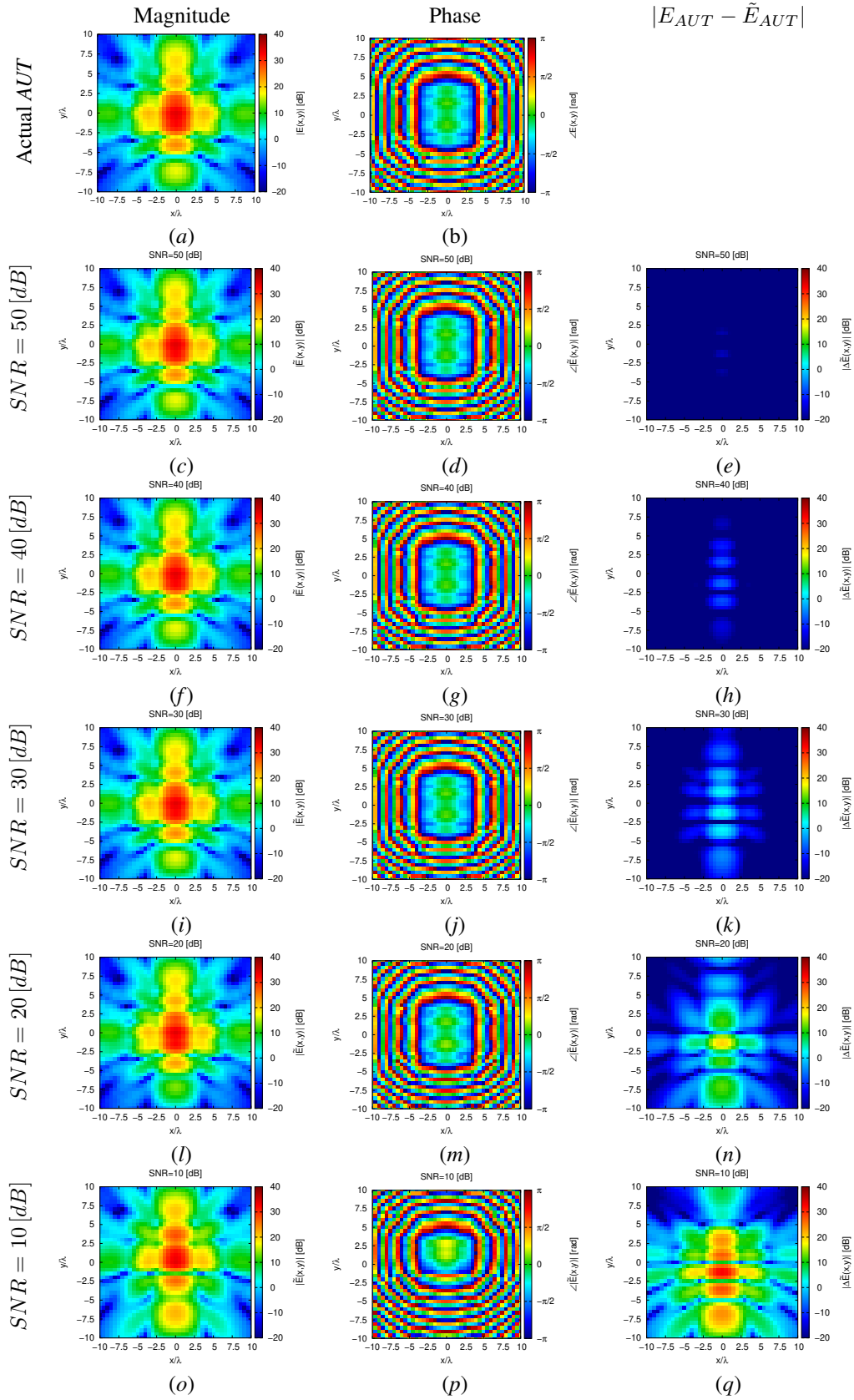


Figure 9: $I = 5$ - Magnitude and phase of the actual and estimated 2 - D near-field pattern when processing noisy measurements at different SNRs.

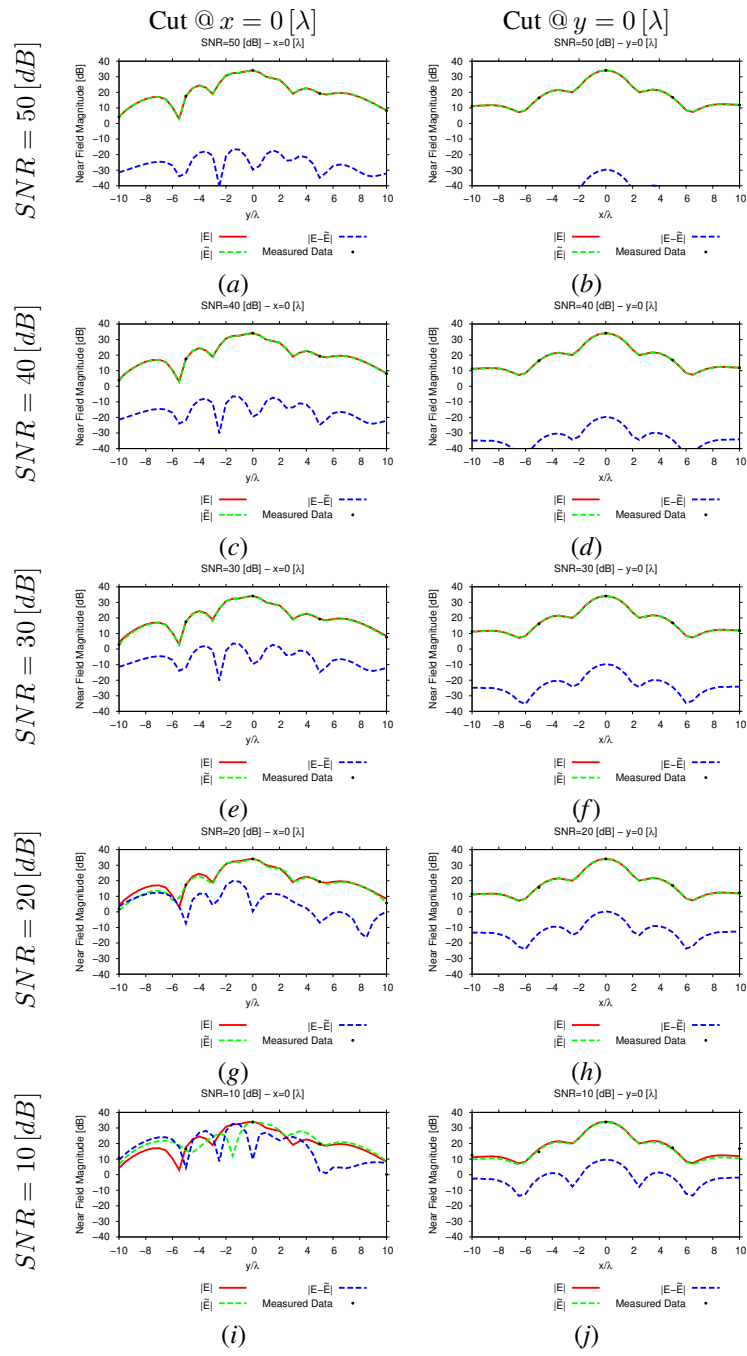


Figure 10: $I = 5 - 1 - D$ cuts of the estimated near-field pattern under several noisy conditions

Estimated Far-Field

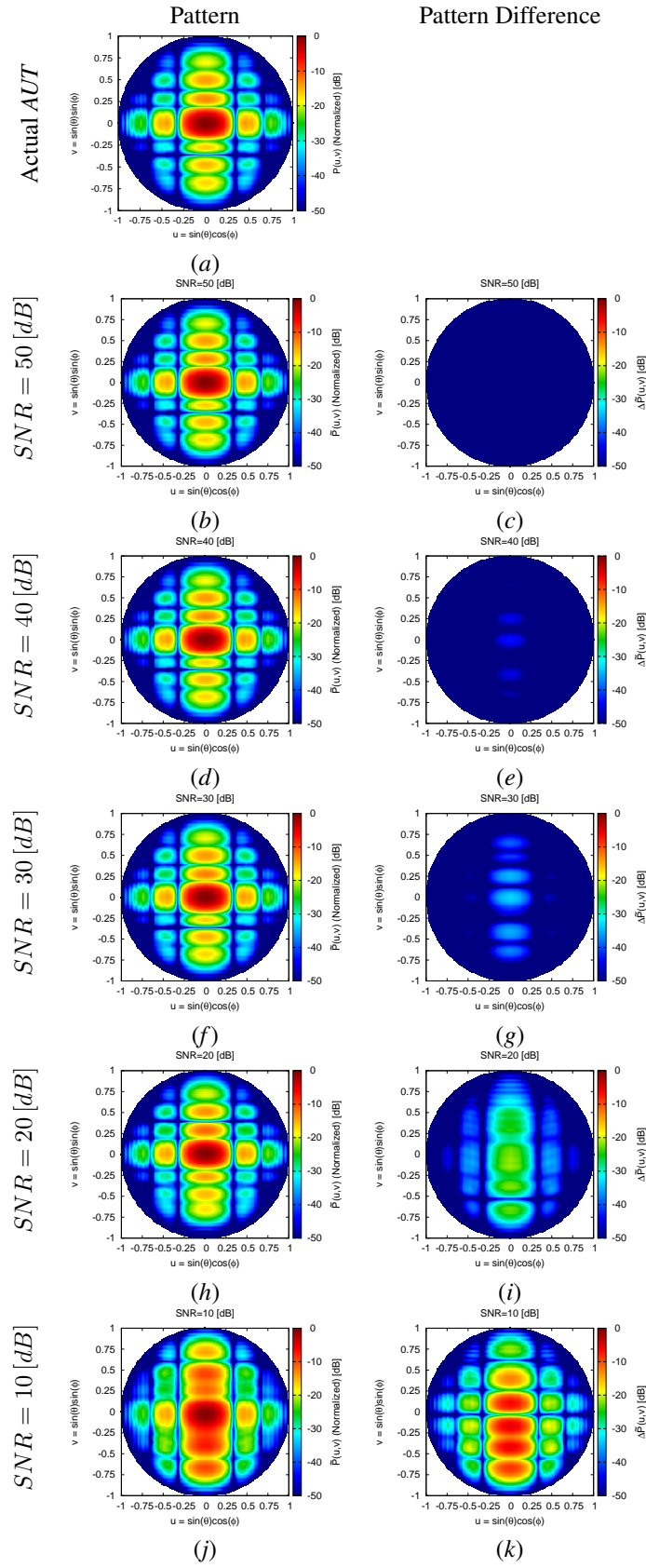


Figure 11: $I = 5$ - Actual and estimated 2 – D far-field patterns at different $SNRs$. All patterns are obtained through near-to-far-field transformation

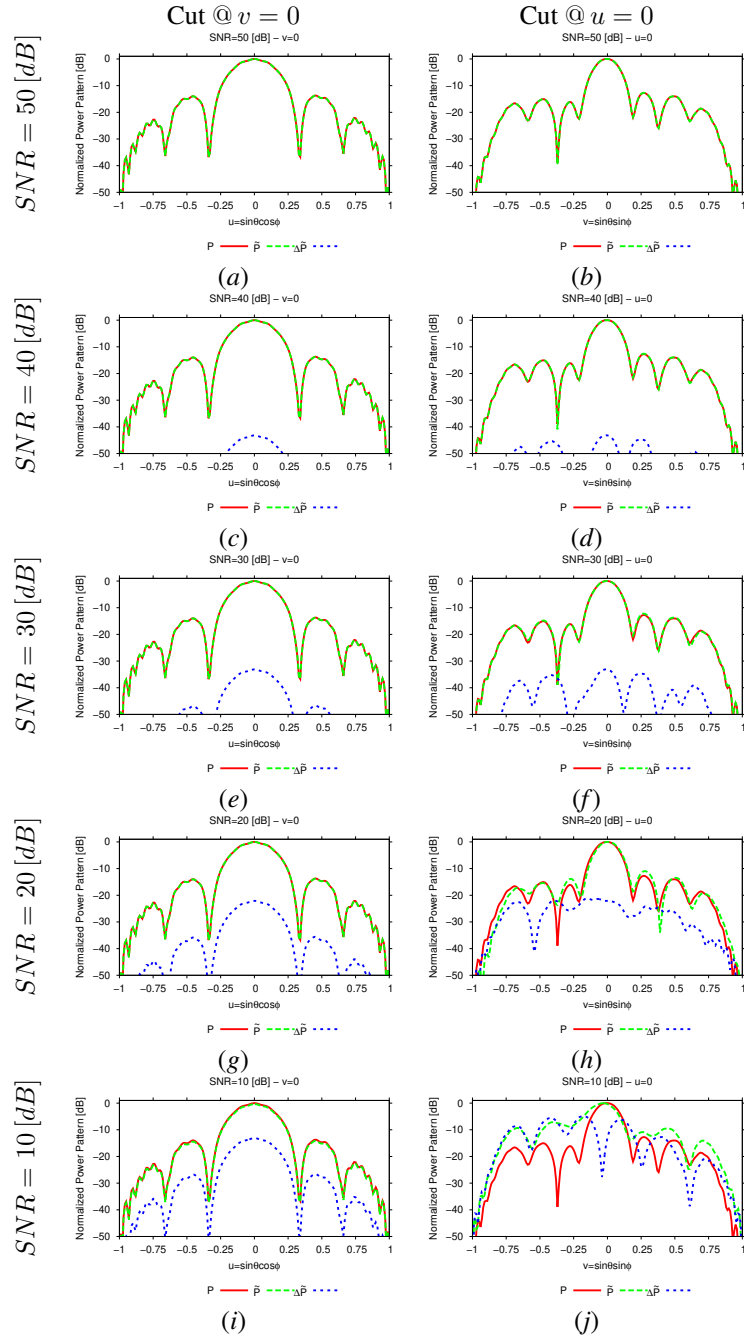


Figure 12: $I = 5 - 1 - D$ cuts of the estimated far-field pattern (obtained through near-to-far-field transformation from the estimated near-field patterns) under several noisy conditions

SNR [dB]	$Far - Field Error, \chi$ [dB]
50	-49.95
40	-39.92
30	-29.86
20	-15.89
10	-1.20

Table II: $I = 5$ - Far-field matching error between the actual and estimated AUT patterns (both obtained through near-to-far-field transformation from the corresponding near-field patterns) under several noisy conditions.

Computational times

- Δt_{Sim} : Time required to simulate the K AUT configurations used to build the $(T \times K)$ "pattern matrix";
- Δt_{SVD} : Time required to perform the SVD of the $(T \times K)$ "pattern matrix";
- Δt_{MbE}^{OMP} : Time required by the Measurement-by-Example tool to read the SVD output and perform the estimation of the AUT radiated field.

$\Delta t_{Sim} [sec]$	2.26×10^4
$\Delta t_{SVD} [sec]$	1.29×10^2
$\Delta t_{MbE}^{OMP} [sec]$	8.00×10^{-3}

Table III: $I = 5$ - Computational times

Remarks

- Given that the number of simulated AUTs is $K = S \times (F^{(3)} + P^{(3)}) = 120$, the average per-AUT simulation time is

$$\Delta t_{FEKO} \simeq \frac{\Delta t_{Sim}}{K} = \frac{2.26 \times 10^4}{120} [sec] = 1.88 \times 10^2 [sec]$$

More information on the topics of this document can be found in the following list of references.

References

- [1] M. Salucci, N. Anselmi, M. D. Migliore, and A. Massa, "A bayesian compressive sensing approach to robust near-field antenna characterization," *IEEE Trans. Antennas Propag.*, vol. 70, no. 9, pp. 8671-8676, Sep. 2022.
- [2] B. Li, M. Salucci, W. Tang, and P. Rocca, "Reliable field strength prediction through an adaptive total-variation CS technique," *IEEE Antennas Wireless Propag. Lett.*, vol. 19, no. 9, pp. 1566-1570, Sep. 2020.
- [3] M. Salucci, M. D. Migliore, P. Rocca, A. Polo, and A. Massa, "Reliable antenna measurements in a near-field cylindrical setup with a sparsity promoting approach," *IEEE Trans. Antennas Propag.*, vol. 68, no. 5, pp. 4143-4148, May 2020.
- [4] G. Oliveri, M. Salucci, N. Anselmi, and A. Massa, "Compressive sensing as applied to inverse problems for imaging: theory, applications, current trends, and open challenges," *IEEE Antennas Propag. Mag.*, vol. 59, no. 5, pp. 34-46, Oct. 2017.
- [5] A. Massa, P. Rocca, and G. Oliveri, "Compressive sensing in electromagnetics - A review," *IEEE Antennas Propag. Mag.*, vol. 57, no. 1, pp. 224-238, Feb. 2015.
- [6] P. Rocca, N. Anselmi, M. A. Hannan, and A. Massa, "Conical frustum multi-beam phased arrays for air traffic control radars," *Sensors*, vol. 22, no. 19, 7309, pp. 1-18, 2022.
- [7] F. Zardi, G. Oliveri, M. Salucci, and A. Massa, "Minimum-complexity failure correction in linear arrays via compressive processing," *IEEE Trans. Antennas Propag.*, vol. 69, no. 8, pp. 4504-4516, Aug. 2021.
- [8] N. Anselmi, G. Gottardi, G. Oliveri, and A. Massa, "A total-variation sparseness-promoting method for the synthesis of contiguously clustered linear architectures," *IEEE Trans. Antennas Propag.*, vol. 67, no. 7, pp. 4589-4601, Jul. 2019.
- [9] M. Salucci, A. Gelmini, G. Oliveri, and A. Massa, "Planar arrays diagnosis by means of an advanced bayesian compressive processing," *IEEE Tran. Antennas Propag.*, vol. 66, no. 11, pp. 5892-5906, Nov. 2018.
- [10] L. Poli, G. Oliveri, P. Rocca, M. Salucci, and A. Massa, "Long-distance WPT unconventional arrays synthesis," *J. Electromagn. Waves Appl.*, vol. 31, no. 14, pp. 1399-1420, Jul. 2017.
- [11] G. Oliveri, M. Salucci, and A. Massa, "Synthesis of modular contiguously clustered linear arrays through a sparseness-regularized solver," *IEEE Trans. Antennas Propag.*, vol. 64, no. 10, pp. 4277-4287, Oct. 2016.
- [12] M. Carlin, G. Oliveri, and A. Massa, "Hybrid BCS-deterministic approach for sparse concentric ring isophoric arrays," *IEEE Trans. Antennas Propag.*, vol. 63, no. 1, pp. 378-383, Jan. 2015.
- [13] G. Oliveri, E. T. Bekele, F. Robol, and A. Massa, "Sparsening conformal arrays through a versatile BCS-based method," *IEEE Trans. Antennas Propag.*, vol. 62, no. 4, pp. 1681-1689, Apr. 2014.

-
- [14] F. Viani, G. Oliveri, and A. Massa, "Compressive sensing pattern matching techniques for synthesizing planar sparse arrays," *IEEE Trans. Antennas Propag.*, vol. 61, no. 9, pp. 4577-4587, Sep. 2013.
- [15] G. Oliveri, P. Rocca, and A. Massa, "Reliable diagnosis of large linear arrays - A bayesian compressive sensing approach," *IEEE Trans. Antennas Propag.*, vol. 60, no. 10, pp. 4627-4636, Oct. 2012.
- [16] G. Oliveri, M. Carlin, and A. Massa, "Complex-weight sparse linear array synthesis by bayesian compressive sampling," *IEEE Trans. Antennas Propag.*, vol. 60, no. 5, pp. 2309-2326, May 2012.
- [17] G. Oliveri and A. Massa, "Bayesian compressive sampling for pattern synthesis with maximally sparse non-uniform linear arrays," *IEEE Trans. Antennas Propag.*, vol. 59, no. 2, pp. 467-481, Feb. 2011.
- [18] P. Rocca, M. A. Hannan, M. Salucci, and A. Massa, "Single-snapshot DoA estimation in array antennas with mutual coupling through a multi-scaling BCS strategy," *IEEE Trans. on Antennas and Propag.*, vol. 65, no. 6, pp. 3203-3213, Jun. 2017.
- [19] M. Carlin, P. Rocca, G. Oliveri, F. Viani, and A. Massa, "Directions-of-arrival estimation through bayesian compressive sensing strategies," *IEEE Trans. Antennas Propag.*, vol. 61, no. 7, pp. 3828-3838, Jul. 2013.
- [20] M. Carlin, P. Rocca, G. Oliveri, and A. Massa, "Bayesian compressive sensing as applied to directions-of-arrival estimation in planar arrays," *J. Electromagn. Waves Appl.*, vol. 2013, pp. 1-12, 2013.
- [21] G. Oliveri, N. Anselmi, M. Salucci, L. Poli, and A. Massa, "Compressive sampling-based scattering data acquisition in microwave imaging," *J. Electromagn. Waves Appl.*, vol. 37, no. 5, pp. 693-729, Mar. 2023.
- [22] G. Oliveri, L. Poli, N. Anselmi, M. Salucci, and A. Massa, "Compressive sensing-based Born iterative method for tomographic imaging," *IEEE Tran. Microw. Theory Techn.*, vol. 67, no. 5, pp. 1753-1765, May 2019.
- [23] M. Salucci, L. Poli, and G. Oliveri, "Full-vectorial 3D microwave imaging of sparse scatterers through a multi-task Bayesian compressive sensing approach," *J. Imag.*, vol. 5, no. 1, pp. 1-24, Jan. 2019.
- [24] M. Salucci, A. Gelmini, L. Poli, G. Oliveri, and A. Massa, "Progressive compressive sensing for exploiting frequency-diversity in GPR imaging," *J. Electromagn. Waves Appl.*, vol. 32, no. 9, pp. 1164-1193, 2018.
- [25] N. Anselmi, L. Poli, G. Oliveri, and A. Massa, "Iterative multi-resolution bayesian CS for microwave imaging," *IEEE Trans. Antennas Propag.*, vol. 66, no. 7, pp. 3665-3677, Jul. 2018.
- [26] N. Anselmi, G. Oliveri, M. A. Hannan, M. Salucci, and A. Massa, "Color compressive sensing imaging of arbitrary-shaped scatterers," *IEEE Trans. Microw. Theory Techn.*, vol. 65, no. 6, pp. 1986-1999, Jun. 2017.
- [27] N. Anselmi, G. Oliveri, M. Salucci, and A. Massa, "Wavelet-based compressive imaging of sparse targets," *IEEE Trans. Antennas Propag.*, vol. 63, no. 11, pp. 4889-4900, Nov. 2015.
- [28] G. Oliveri, P.-P. Ding, and L. Poli "3D crack detection in anisotropic layered media through a sparseness-regularized solver," *IEEE Antennas Wireless Propag. Lett.*, vol. 14, pp. 1031-1034, 2015.

-
- [29] L. Poli, G. Oliveri, P.-P. Ding, T. Moriyama, and A. Massa, "Multifrequency Bayesian compressive sensing methods for microwave imaging," *J. Opt. Soc. Am. A*, vol. 31, no. 11, pp. 2415-2428, 2014.
- [30] G. Oliveri, N. Anselmi, and A. Massa, "Compressive sensing imaging of non-sparse 2D scatterers by a total-variation approach within the Born approximation," *IEEE Trans. Antennas Propag.*, vol. 62, no. 10, pp. 5157-5170, Oct. 2014.
- [31] L. Poli, G. Oliveri, and A. Massa, "Imaging sparse metallic cylinders through a local shape function bayesian compressive sensing approach," *J. Opt. Soc. Am. A*, vol. 30, no. 6, pp. 1261-1272, 2013.
- [32] L. Poli, G. Oliveri, F. Viani, and A. Massa, "MT-BCS-based microwave imaging approach through minimum-norm current expansion," *IEEE Trans. Antennas Propag.*, vol. 61, no. 9, pp. 4722-4732, Sep. 2013.
- [33] F. Viani, L. Poli, G. Oliveri, F. Robol, and A. Massa, "Sparse scatterers imaging through approximated multitask compressive sensing strategies," *Microwave Opt. Technol. Lett.*, vol. 55, no. 7, pp. 1553-1558, Jul. 2013.
- [34] L. Poli, G. Oliveri, P. Rocca, and A. Massa, "Bayesian compressive sensing approaches for the reconstruction of two-dimensional sparse scatterers under TE illumination," *IEEE Trans. Geosci. Remote Sensing*, vol. 51, no. 5, pp. 2920-2936, May 2013.
- [35] L. Poli, G. Oliveri, and A. Massa, "Microwave imaging within the first-order Born approximation by means of the contrast-field Bayesian compressive sensing," *IEEE Trans. Antennas Propag.*, vol. 60, no. 6, pp. 2865-2879, Jun. 2012.
- [36] G. Oliveri, L. Poli, P. Rocca, and A. Massa, "Bayesian compressive optical imaging within the Rytov approximation," *Optics Letters*, vol. 37, no. 10, pp. 1760-1762, 2012.
- [37] G. Oliveri, P. Rocca, and A. Massa, "A Bayesian compressive sampling-based inversion for imaging sparse scatterers," *IEEE Trans. Geosci. Remote Sensing*, vol. 49, no. 10, pp. 3993-4006, Oct. 2011.